Widespread Decline in Terrestrial Water Storage and Its Link to Teleconnections across Asia and Eastern Europe

Xianfeng Liu[1,2], Xiaoming Feng[1], Philippe Ciais[3], Bojie Fu[1]

[1]State Key Laboratory of Urban and Regional Ecology, Research Center for Eco-Environmental Sciences, Chinese Academy of Sciences, Beijing 100085, China
[2]School of Geography and Tourist, Shaanxi Normal University, Xi'an 710119, China
3Laboratoire des Sciences du Climat et de l'Environnement, CEA-CNRS-UVSQ, Gif-sur-Yvette, France

Correspondence to: Xiaoming Feng (fengxm@rcees.ac.cn)

Abstract. Recent global changes in terrestrial water storage (TWS) and associated freshwater availability raise major concerns over the sustainability of global water resources. However, our knowledge regarding the long-term trend in TWS and its components is still not well documented. In this work, we characterize the spatiotemporal variations in TWS and its components over the Asian and Eastern European regions during the period of April 2002 to June 2017 based on the Gravity Recovery and Climate Experiment (GRACE) satellite observations, land surface model simulations and precipitation observations. The connections of TWS and global major teleconnections (TCs) are also discussed. The results indicate a widespread decline in TWS during 2002-2017, and five hotspots of TWS negative trends were identified with trends between -8.94 mm yr^{-1} and -21.79 mm yr^{-1}. TWS partitioning suggests that these negative trends are primarily attributed to the intensive overextraction of groundwater and warm-induced surface water loss, but the contributions of each hydrological component vary among hotspots. The results also indicate that the El Niño-Southern Oscillation, Arctic Oscillation and North Atlantic Oscillation are the three largest, dominant factors controlling the variations in TWS through the covariability effect on climate variables. However, seasonal results suggest a divergent response of hydrological components to TCs among seasons and hotspots. Our findings provide insights into changes in TWS and its components over the Asian and Eastern European regions, where there is a growing demand for food grains and water supplies.

1 Introduction

Terrestrial water storage (TWS), a fundamental component of terrestrial hydrological cycles (Tang et al., 2010), represents the total water stored above and below the land surface (Syed et al., 2008). TWS was composed of surface water (SW), including lakes, snow water equivalent, canopy water and glaciers, soil moisture (SM) and groundwater (GW) storage (Cao et al., 2019;Ni et al., 2018). Recent TWS has raised worldwide concerns because of its association with freshwater availability and concerns of the sustainability of global water resources (Creutzfeldt et al., 2012; Meng et al., 2019). Moreover, the GRACE (Gravity Recovery and Climate Experiment) satellites provided measurements of global TWS changes from April 2002 to June 2017 (Reager et al., 2009), which provided hydrologists with practical insights at regional

and global scales in comparison to in situ measurements (Cao et al., 2019; Zhang et al., 2015). With GRACE data, previous literature mostly focus on the TWS changes at the basin or regional scale (Creutzfeldt et al., 2015; Long et al., 2013; Ndehedehe et al., 2017; Ni et al., 2018; Rodell et al., 2009; Shamsudduha et al., 2017; Syed et al., 2008; Yang et al., 2017; Yi et al., 2016; Zhang et al., 2015). GRACE data also contributes to the exploration of hydrological storage changes, e.g.,

35 glacial mass loss (Brun et al., 2017; Huss et al., 2018; Jacob et al., 2012), lake level and extent changes (Zhang et al., 2017; Zhang et al., 2013) and groundwater depletion (Feng et al., 2018; Long et al., 2016; Rodell et al., 2009; Wada et al., 2010). However, limited works have focused on the contributions of TWS components at a large scale, particularly in water-limited and densely populated regions (Tapley et al., 2019), until two recent global scale studies significantly improved our knowledge by identifying 34 hotspots of TWS changes during 2002-2016 (Rodell et al., 2018) and the changes in global

40 endorheic basin water storage (Wang et al., 2018).

The Asian and Eastern European regions, home to half of the world's population and 50% of the arid/semiarid climate areas, is undergoing intensive water threats to agriculture and domestic water needs (Huang et al., 2016) (Figure 1). Most of the countries located on the borders of Asia and Eastern Europe are experiencing water resource shortages owing to low annual precipitation (less than 400 mm/y), which consequently forms the largest amount of irrigated land in the world (Rodell et al.,

45 2009). The increasing demand for freshwater and the limited knowledge on the available water resources in this region have become the key challenges to achieving sustainability in these areas (Feng et al., 2013). Therefore, knowledge on the TWS trend and its hydrological components is important for sustainable development of water resource and food supply in this region (Rodell et al., 2018).

The large-scale mode of teleconnection (TC) is an overwhelming factor of regional water resources, modulating the location

50 and strength of storm tracks and fluxes of heat, moisture and momentum. For example, prominent teleconnection patterns such as El Niño-Southern Oscillation (ENSO) show that El Niño years are related to reduced precipitation, continental freshwater discharge, and evapotranspiration on land, and therefore, TWS variability occurs over many land areas (Gonsamo et al., 2016). Many studies have invested their efforts to address the possible causes of TWS changes by connecting TWS with TC (Ndehedehe et al., 2017; Ni et al., 2018; Phillips et al., 2012). However, these studies focused primarily on the

55 effect of ENSO on TWS. Notably, many other global and regional climate TCs also influence the changes in TWS, which has been less documented and consequently limits our understanding of a comprehensive TWS-TC correlation. Therefore, knowledge of the influence of multiple TCs on TWS is critical to improve our understanding and properly manage water resources (Ndehedehe et al., 2017; Phillips et al., 2012).

Here, we conduct a comprehensive analysis of the spatiotemporal variations in TWS across the Asian and Eastern European

60 regions and address the contributions of each hydrological component and connection with TCs using multisource data. First, we calculate the deseasonalized trend and analyse the spatiotemporal variations in TWS across Asia and Eastern Europe. Then, we partition the components of TWS into SW, SM and groundwater by using GRACE, land surface model and lakes and glacial observation data. Finally, we calculate the cross-correlation coefficients between TCs and the remainder of the TWS time series. We aim to explore 1) the spatial pattern of long trends in TWS, 2) the contributions of water components

65   to TWS variations among regions, and 3) the role of TCs in the changes in TWS and its components over Asian and the
Eastern European regions.

2 Materials and Methods

2.1 Study area

The Asian and Eastern European regions are located between latitudes 6°S and 56°N and longitudes 4°E and 109°E. These
70   regions comprise highly populated lands that vary spatially in climate, topography and hydrology. A total of 54% of the area
is arid and semiarid (Figure 1a). The topography is dominated by plains, plateaus, and mountains such as the Himalaya
Mountains, the Tien Shan Mountains, the Gangetic Plains, the Loess Plateau, and Mount Kilimanjaro. More importantly, the
Asian and Eastern European regions are the most densely populated regions in the world (available at
http://sedac.ciesin.columbia.edu/data/ collection/gpw-v4), sustaining nearly half of the total population of the world and
75   contain the largest, most intensively irrigated land in this area (Figure 1b). Under the combined effect of climate change and
anthropogenic activities, the amount of sustainable available freshwater has become increasingly dire for food and water
security and hence sustainable social economies.

2.2 Data

In this work, both of the mass concentration (mascon) solutions, including the Jet Propulsion Laboratory (hereafter JPL-M)
80   (Watkins et al., 2015) and Center for Space Research (CSR-M) (Save et al., 2016) datasets were used to detect TWS changes
across the Asian and Eastern European regions with spatial resolutions of 0.5° × 0.5° for the period between April 2002 and
June 2017 for a total of 183 solutions. The 20 months of missing data in the original time series were filled by the linear
interpolation method (Long et al., 2015;Yang et al., 2017). The GRACE anomalies reported in these mascon solutions are
relative to a 2004-2009 mean baseline (Scanlon et al., 2016). For details on the data processing, readers are referred to Save
85   et al. (2016) and Watkins et al.(2015) for the mascon solutions.

The Global Land Data Assimilation System (GLDAS) was used to partition the GRACE-observed TWS changes into SW
(snow water equivalent, canopy water, lakes and glaciers), SM and groundwater (Rodell et al., 2004). The monthly data
products from the GLDAS version 2.1 Noah model contain thirty-six parameters, including canopy water storage, snow
water equivalent and SM data. Noah has a total of 4 layers of SM thickness: 0-10, 10-40, 40- 100, and 100-200 cm. To
90   compute the Noah TWS, the SM in all layers, snow water equivalent, and canopy SW are summed. In this study, the
monthly canopy water storage, snow water equivalent and SM data were obtained from GLDAS version 2.1 with a spatial
resolution of 0.25° × 0.25° during 2002 and 2017 (available at https://disc.gsfc.nasa.gov/datasets?page=1&project =GLDAS).
Then, we resampled these data to a 0.5° × 0.5° spatial resolution using the bicubic method prior to the analysis.

The integrated total water content, which is obtained from the GLDAS output by summing the layers of canopy water
95   storage, four SM layers and snow equivalent water, is directly comparable to that which GRACE measures over land, and

users need to be aware that the GLDAS version used here does not include groundwater and separate SW components (such as rivers and lakes). Thus, deviations from the GRACE total water storage changes can be expected. The comparison between GRACE and GLDAS is shown in Figure S1. Lake level data derived from multimission altimeter observations were obtained from the Database for Hydrological Time Series of Inland Water (Schwatke et al., 2015) and Hydroweb (Crétaux et

100 al., 2011). Glacier mass change data are available from the published literature (Brun et al., 2017; Wang et al., 2018). The groundwater counterpart was estimated by deducted the estimated SW and SM changes from the GRACE-observed TWS change (Wang et al., 2018). Notably, interannual variations in biomass have been shown to be well below the detection limits of GRACE (Rodell et al., 2005; Rodell et al., 2009); therefore, the variability in SW counterpart mainly involves changes in lakes, snow and ice in this study.

105 To investigate the effects of TCs on the changes in TWS across Asia and Eastern Europe, 12 popular annual TC indices that influence the Northern Hemisphere and global climate were included, namely, Arctic Oscillation (AO), North Atlantic Oscillation (NAO), East Atlantic (EA), East Atlantic/Western Russia (EAWR), Scandinavia (SCAND), Polar/Eurasia (polarEA), West Pacific (WP), Pacific/North America (PNA), Indian Ocean Dipole (IOD), Atlantic Multidecadal Oscillation (AMO), Pacific Decadal Oscillation (PDO), and ENSO (Zhu et al., 2017). All of these indices were obtained from the

110 Climate Prediction Center of the U.S. National Oceanic and Atmospheric Administration.

2.3 Methods

2.3.1 Time series decomposition

The deseasonalized time series was used to calculate the TWS trend by Sen linear regression. The original TWS signal is decomposed into long-term trends, seasonality signals, and residual components by implementing the Seasonal

115 Decomposition of Time Series by Loess (STL) approach. The residuals (total-trend-seasonality) are used to calculate the cross-correlation between the TWS and TC indices to partly reduce the interference with glacier melt and anthropogenic activities, i.e., TWS and TC indices, groundwater withdrawal for irrigation, mining, and human-made reservoirs for water resource management (Humphrey et al., 2016). The STL method is a robust method for detecting nonlinear time series in trend estimates, and the equation is as follows:

120
$$S_{total} = S_{long-term} + S_{seasonality} + Residuals \,, \tag{1}$$

where S_{total} is the original signal, $S_{long-term}$ is the long-term trend, $S_{seasonality}$ is the seasonality signal and *Residual* is the residual component. We also provide an example for the TWS time series and its decomposition components in Figure S2. For detailed principles and applications of STL, readers are encouraged to refer to (Bergmann et al., 2012; Cleveland et al., 1990).

2.3.2 Theil-Sen trend analysis

We calculated the linear rates of TWS and precipitation change for the Asian and Eastern European regions from April 2002 to June 2017 using the Theil-Sen trend method (Sen, 1968) and tested the significance of the trend using the Mann-Kendall statistical test (Kendall, 1955). The advantage of the Theil-Sen trend is that it is nonsensitive to outliers and therefore can be more accurate than a simple linear regression for skewed and heteroscedastic data. This method competes well against the non-robust least squares method even for normally distributed data. The TWS trend β for a particular pixel is as follows:

$$\beta = \text{Median}\left(\frac{x_j - x_i}{j - i}\right), \forall \, j > i, \tag{2}$$

where i,j are the time series sequences and x_i, x_j are the TWS values at times i,j. When β>0, the TWS in the corresponding pixel reveals an increasing trend; when β<0, the TWS in this pixel reveals a decreasing trend.

2.3.3 Cross-correlation analysis

Contemporaneous weather conditions impact TWS, often with evident time lags. Therefore, in this paper, we employ the cross-correlation method to explore the relationship between TWS and teleconnection indices. The cross-correlation measures the similarity of the two time series datasets as a function of the displacement of one set relative to the other (Oppenheim et al., 2009). The cross-correlation is defined as follows:

$$\rho(\tau) = \frac{\sigma_{12}(\tau)}{\sqrt{\sigma_{11}\sigma_{22}}}, \tag{3}$$

where $\sigma_{12}(\tau)$ is the cross-covariance function of x_1 (t) leading the lagged x_2 (t), and σ_11 and σ_22 represent the auto-variances of x_1 (t) and x_2 (t), respectively. Moreover, we focus on the current and historical influence of TCs on TWS changes, and hence, we constrain that the value of ρ(τ) lies between 0 and 24 (Ni et al., 2018). Higher cross-correlation values indicate a stronger influence of a TC on TWS and its components. Spatially, we calculated the cross-correlation at the residual time series (full signal -(long-term trends + seasonality cycle)) to partially remove the influence of unaccounted factors on TWS changes, assuming that the trend was mainly induced by secular climate change or direct human impacts rather than interannual climate variability (Phillips et al., 2012; Wang et al., 2018).

3 Results

3.1 Spatiotemporal changes in TWS

JPL-M indicates that the Asian and Eastern European regions experienced widespread decline in TWS during 2002-2017 (Figure 2a). Noticeably, the spatial regime of the TWS variation matches that of the trend in precipitation, except for northwest India, north and east of the Caspian Sea, and north of Xinjiang in China (Figure 2b), suggesting that variations in TWS in these regions are intertwined with human impacts. Spatially, five hotspots of TWS decline were identified (Figure 2f, Figure S6 and Table S1). The North China Plain (Region 1), a vast agricultural region in China, has undergone a

continuously negative trend in TWS (-8.94 ± 3.91 mm y^{-1}), although an increasing trend in precipitation is expected in the

155   northern part of this region (Figure 2c). Another hotspot of TWS decline is located west of Urumqi in the China's northwestern Xinjiang Province (Region 2), with a negative trend of -15.93 ± 11.58 mm y^{-1}. Rainfall in this region shows an increasing trend during the study period (Figure 2c). The most striking TWS deficit is in northwest India (Region 3 in Figure 2a, -21.79 ± 14.54 mm y^{-1}), which is within (Rodell et al., 2009) 40 ± 10 mm y^{-1} during 2002-2008. The difference may stem from the differences in spatial boundaries and time spans. Two subcentres of TWS deficits (-11.74 ± 8.11 mm y^{-1}) are located

160   at the border of China, India, Bhutan and Nepal (Region 4 in Figure 2a). The Middle East region witnessed the most widespread TWS depletion (-10.93 ± 7.91 mm y^{-1}) in the study area (Region 5), and the Caspian Sea level showed a dramatically negative trend (-73.2 mm y^{-1}) during the GRACE era (Figure S3).

There are also several regions with increased TWS. For example, South China experienced an increasing TWS trend during 2002-2017. Another wet centre in China is located in the hinterlands of the Tibetan Plateau. Increasing precipitation and

165   warming-induced glacial loss led to an expansion of lake in the Inner Tibetan Plateau and may be a recharge source for TWS (Huss et al., 2018; Brun et al., 2017; Wang et al., 2018). TWS in central and southern India exhibits an increasing trend during 2002-2017. The variability in southern monsoons and the associated increase in rainfall likely account for the positive trend in TWS (Figure 2b). Other regions with increased TWS are in Russia and northeast China, coinciding with an increase in precipitation in those regions during the study period. Based on the above analysis, we can conclude that the scattered

170   positive TWS trends mostly correlate with natural variability, i.e., precipitation increases. Notably, although in a smaller trend, the results of CSR-M followed the spatial and temporal pattern of JPL-M (Figure S4), further strengthening the robustness of our results.

3.2 Influence of TC indices on TWS variability

Figure 2 and Figure S5 show the spatial distribution of the cross-correlation coefficients, illustrating the possible relationship

175   of TCs with interannual variability in TWS. The results indicate that ENSO, AO and NAO have a comparable area percentage (more than 20% of the study area) in influencing TWS variability. Spatially, the pattern of correlation coefficients between TWS and ENSO is heterogeneous, with positive correlations mostly in southeast China and boreal regions and negative correlations in southeast Asia, India, and eastern boreal regions (Figure S5). The second and third dominant teleconnection modes are AO and NAO, respectively. AO mainly affects TWS variations across high-latitude

180   regions through its impact on temperature variability, and NAO has a wider footprint that is scattered across the whole study. Following the three dominant TCs. The effects of IOD are scattered throughout south India, southeast Asia, the Yellow River basin, and the Euro boreal region. Most regions in the low latitudes show a negative correlation between TWS and IOD and a positive correlation in the high latitudes. Other teleconnection modes typically have a smaller impact on TWS dynamics over the study area.

185   Our results also indicate a remarkable time-lagged effects of TCs on the variations in TWS (Figure 2d). Nearly half of the area (49.14%) lags behind the TCs by up to 3 months, while the proportions of TWS variations lagging behind the TCs at (4-

6 months) and at (7-9 months) are 20.27% and 12.28%, respectively. These time lags are mainly scattered in the mid-high-latitude region and the Yangtze River basin in China. Longer lags (10-18 months), accounting for 18.31%, are observed in parts of Southeast Asia and the Middle East region. Proportions of time lags for different TCs are shown in Figure 2d.

190   Notably, the spatial pattern of the dominant TC having only a limited extent with respect to their influence on climate conditions. The heterogeneous pattern highlighted the importance of focusing on the effect of multiple TCs on TWS rather than one teleconnection index.

3.3 Contributions of water storage components to TWS

TWS variations during 2002-2017 contributed differently to SW (lakes, biomass, snow, and ice), SM and groundwater

195   (Figure 3) among the five hotspot regions (circled in Figure 2a). Groundwater depletion dominance (-8.68±2.89 mm y^{-1}) compared to TWS loss is observed in region 1 compared to the other two components (-0.27±2.97 mm y^{-1} for SM, 0.02±0.11 mm y^{-1} for SW) during the study period. Similarly, a more prominent of groundwater depletion than TWS loss is also observed in northwest India (region 3 with -21.35 mm y^{-1}), which experienced the most extensive land irrigation worldwide (Figure 1b). The contributions of the SW and soil water in the above two regions are very small and neglected. The rapid

200   glacial mass loss in the Tien Shan Mountain range induced a 41% water loss (Brun et al., 2017; Jacob et al., 2012). The melt water could replenish the soil water, leading to an increase in soil water components (2.18±2.82 mm y^{-1}) in northwest China (region 2) (Figure 3). Notably, irrigated agriculture is the major style of agricultural development in this region (Yang et al., 2017), which contributes to more than half (-11.61±13.02 mm y^{-1}) of the total water loss. Both groundwater depletion and glacial melt may enhance evapotranspiration by pumping water from aquifers and mountains to the surface, which induces a

205   decline in TWS (Thomas et al., 2014; Wang et al., 2018). The contributions of the fourth region are 2.48±1.81 mm y^{-1}, -3.22±7.24 mm y^{-1} and -11.00±10.43 mm y^{-1} for SW, SM and groundwater, respectively, suggesting that groundwater withdrawal is the primary reason for TWS depletion. This region is also spatially coherent with precipitation deficits, as depicted in Figure 2b, particularly in the eastern part of this hotspot, accentuating the impact of meteorological drought on TWS. The prominent SW loss (-3.83±1.68 mm y^{-1}) in the fifth region can be attributed to the sharply shrinkage in the

210   Caspian Sea with a decrease in sea level of -73.2 mm y^{-1}, which is comparable to -68 mm y^{-1} during 2002-2016 (Wang et al., 2018). The dramatic decline in the Caspian Sea level contributes to a third of the total TWS loss in this region. The large decrease in TWS in these areas can also be attributed to the heavy reliance on groundwater for irrigation and domestic needs due to the construction of dams upstream (Voss et al., 2013; Rodell et al., 2018). The slight decreasing trend in precipitation and associated droughts will significantly exacerbate the TWS depletion, as the recharge of TWS relies largely on

215   precipitation in those water-limited regions.

3.4 Divergent response of water storage components to TCs

Our results indicate that the water storage components are simultaneously influenced by several teleconnection. For instance, SM in region 2 significantly correlates with NAO, AO, EAWR, PNA, ENSO, IOD, EA, AMO, polarEA and PDO, with

negative correlations for some indices and positive correlations with others. Hence, the dominant teleconnection varies for
220   different water storage components among the regions (Table S2). For each component, TWS and groundwater are generally
less sensitive to TC signals compared to the surface and SM counterparts (Table S3). A possible explanation may be that
TWS is a synthesis signal that its trend will be offset by its components in different ways, and the groundwater intensively
interferes with anthropogenic activities such as irrigation by groundwater withdrawal, which indicates less correlation with
TCs.

225   Further seasonal analysis indicates that the response of water storage to TCs is seasonally different from one region to
another. For example, TC signals have a dominant control on TWS and component variability in spring and summer for
region 3 and region 1, respectively, whereas TC signals control more of the changes in SM in region 5 in autumn and winter.
Notably, although it has been well documented that the dramatic decline in TWS in northwest India can be attributed to the
overexploitation of groundwater (Rodell et al., 2009), our seasonal response of water components to TCs suggests that the
230   SM in this region is highly correlated with spring ENSO signals (Figure 4, r = 0.71). These results highlight the importance
of understanding the seasonal responses to TCs to improve the understanding and prediction of changes in TWS and
associated water storage components.

4 Discussion

4.1 Comparison of our results to previous studies

235   We investigated the spatiotemporal trend of TWS and its components over Asia and Eastern Europe during 2002-2017. The
overall pattern and trend of TWS over the study area are consistent with those of previous studies (Humphrey et al., 2016;
Scanlon et al., 2016). In region 1, our estimate is within that of previous studies in this region (22±3 mm y-1 during 2003-
2010) (Feng et al., 2013). Due to a long-term warm and dry climate and intensive anthropogenic activities (agriculture,
industry, and urbanization), the groundwater in the region has been overexploited since the 1970s, and more than 70% of the
240   groundwater exploitation is used for regional irrigation (Wang et al., 2007). The glaciers of Tien Shan Mountain are melting
rapidly (-0.28±0.20 m w.e.yr-1) (Jacob et al., 2012), accelerating an increase in the loss of water resources since the glacial
meltwater will provide additional water that was lost to rivers or evaporation. Therefore, the negative trend in TWS indicates
that water demand is larger than supply in region 2, which can be attributed to both continuous withdrawal of groundwater
and extensive evaporation in the endorheic basin (Rodell et al., 2018). The increase in precipitation is expected to offset a
245   certain portion of water losses in this region. In region 3, the rate of groundwater loss was also reported by a previous study
(approximately 40±10 mm y-1 from August 2002 to October 2008) (Rodell et al., 2009). As Indian agriculture leads the
world in total irrigated land by consuming ~85% of the utilizable water resources (Panda et al., 2016; Salmon et al., 2015), a
concluding consensus has been reached that the dramatic decline in TWS is mainly due to the overexploitation (extraction
exceeding recharge) of groundwater for irrigation (Shamsudduha et al., 2019). Although precipitation in this region shows an
250   increasing trend during the GRACE period, the rapid depletion of TWS in northwest India induced by unsustainable

consumption of groundwater for irrigation and other anthropogenic uses has attracted worldwide attention because it is a major threat to India's sustainability (Panda et al., 2016; Rodell et al., 2009). Region 4 in our study is also heavily irrigated (Figure 1), so intensive irrigation is likely to induce groundwater decline. The increase in SW induced by melt water from mountains (Brun et al., 2017) was offset by the decrease in soil water that may be related to the decrease in precipitation

255 (Figure 2b). In addition to the water body loss, the overreliance on groundwater for domestic and agricultural needs was also identified due to human-made dams influencing region 5 (Joodaki et al., 2014; Rodell et al., 2018; Voss et al., 2013), which is consistent with our results.

Notably, our study focused primarily on a water storage deficit hotspot analysis, which is free of bias compared to that obtained by the whole basin-based evaluation, where basins that experience both drying and wetting trends in the different

260 sub-basins contribute to the calculation of the basin average TWS (Sun et al., 2018). Additionally, previous studies mainly focused on the influence of ENSO on TWS (Ni et al., 2018; Phillips et al., 2012), and we provide a comprehensive analysis of 12 commonly used teleconnection indices and suggest that dominant TCs vary considerably for each component and region. Any conclusions or predictions of TWS and component variability based solely on TCs should be approached with caution, and multiple TCs are strongly recommended to explain the changes in TWS and its components.

265 **4.2 Possible mechanisms of TC influence on TWS variability**

Periodic variability in the climate system can strongly influence regional meteorological patterns and the associated TWS. Unlike a single meteorological variable, teleconnection patterns control heat, moisture, and momentum balances through their effects on temperature, precipitation, and solar radiation reaching the Earth's surface. Therefore, the inherent mechanisms of the TC's influence on TWS variations are related to the combined simultaneous effects of TCs on regional

270 climate factors (precipitation, temperature, and radiation); the changes in climate factors will significantly affect the recharge (precipitation) and loss (evapotranspiration) of regional water resources, which eventually influences the changes in TWS. This mechanism is also documented in former works (Ni et al., 2018; Zhu et al., 2017). We have identified several dominant TCs that influence the variability in TWS and its components. For example, during positive ENSO phases, warmer and drier conditions over India and southeast Asia are associated with a decrease in TWS. When the AO index is positive and the

275 vortex is intense, the winds tighten like a noose around the North Pole, locking cold air in place and contributing to the unusual warmth over the Northern Hemisphere land masses. The positive phase of the NAO, which is highly correlated with AO (r = 0.64, p < 0.01), leads to an intensification of the west wind drift due to a reinforcement of the Iceland low and the Azores high pressure systems, which particularly apparent in the boreal winter months (Wallace et al., 1981). In turn, this results in positive precipitation anomalies in central Europe and negative anomalies in southern Europe and on the

280 Norwegian coast, which is reflected in the water storage variations. IOD is similar to ENSO and often co-occurring with ENSO (Du et al., 2009). During the positive IOD phase, anomalous cool (warm) waters appear in the eastern (western) Indian Ocean in association with large-scale circulation changes that bring anomalous dry conditions to Indonesia, while East Africa experiences above-average rainfall (Webster et al., 1999). These results imply that climate variability may exert

important influences on the TWS, which is generally consistent with the existing literature (Ni et al., 2018; Phillips et al.,
285   2012; Zhang et al., 2015). However, challenges remain in separating the long-term relative roles of natural climatic variation
and anthropogenic forcings on TWS changes.

4.3 Implications for future hydrological studies

Our results indicate that climate variability could explain the increase in TWS and the decrease in most remote and sparsely
populated regions. To a certain extent, climate variability could also indirectly explain glacial melt-induced changes in TWS,
290   such as warming-induced glacial retreat. However, climate variability will interact with human activities, i.e., groundwater
abstraction, in regions with intensive human activities. Although we could obtain the contributions of different water storage
components (SW, SM, and groundwater) through TWS partitioning, each component also influences both climate variability
and human activities, which makes it extremely complicated to elicit the contribution of climate change and other processes.
Thus, well-designed experiments and coupled human-natural system models are still needed to clarify the quantitative
295   contributions of each influencing factor on TWS and its component variability. However, our study provides a new view of
teleconnections to better understand the changes in TWS, enriching the limited knowledge pool of TWS dynamics
attributions. Notably, we claim that climate variability-induced extremes, such as drought and heatwaves, will exacerbate the
TWS loss through increased consumption of water resources from groundwater for irrigation and human water demand in
these hotspots, rather than climate variability alone causing the observed TWS loss.

300   There are several recommendations for future hydrological studies. First, withdrawal of freshwater from groundwater in
water-limited regions is important for sustainable development of water resource and food supply (Rodell et al., 2018).
However, groundwater drought is a distinct class of drought resulting from a decrease in groundwater storage (Thomas et al.,
2017). Understanding groundwater drought is important in water-limited regions where the interplay between groundwater
recharge and abstraction results in variable groundwater stress conditions. GRACE has the unique potential to obtain data on
305   groundwater storage by introducing subsidiary datasets. Second, glacier mass loss in mountainous areas can not only relieve
drought stress in drought years (Huss et al., 2018) but also results in hydroclimatic extremes, e.g., floods. Neither of these
phenomena can be detected using only precipitation datasets, such as those commonly used in monitoring drought and flood
events (Sherwood et al., 2014), which highlights the importance of TWS-related hydroclimatic extremes. With the release of
the GRACE follow-up satellite (Famiglietti et al., 2013), consecutive prolonged data records could provide valuable solution
310   for evaluating hydrological conditions from a long-term perspective and would lead to considerable improvements in our
knowledge of TWS-related hydroclimatic extremes (Famiglietti et al., 2013). Third, a recent study found that the CO_2
growth rate is strongly sensitive to observed changes in TWS (Humphrey et al., 2018), and the coupling between the water
and carbon cycles highlights the need for stronger interactions between the hydrological and biogeochemical research
communities to achieve sustainable development of the Earth system.

5 Conclusions

In this study, we characterize the spatiotemporal variations in TWS and its components and connect these variations with TCs over the Asian and Eastern European regions from April 2002 to June 2017 using multiple sources of data. The results indicate a widespread decline in TWS during 2002-2017, and five hotspots of TWS negative trends were identified with trends between -8.94 mm y-1 and -21.79 mm y-1. Partitioning of TWS suggests that these negative trends are mainly attributed to intensive groundwater extraction and warming-induced SW loss, but the contributions of each hydrological component vary among regions. The results also indicate that ENSO, AO and NAO are the largest three dominant factors in controlling variations in TWS through their covariability effects on climate variables. However, seasonal results suggest a divergent response of hydrological components to TCs among seasons and regions, highlighting the importance of knowledge of the seasonal responses to TCs to improve the understanding and prediction of changes in TWS and associated water storage components. Our study provides a comprehensive analysis of TWS variability and its connection to TCs across the Asian and Eastern European regions, facilitating the target strategy of water resource management.

Data availability

The data and code generated in this study are available from the authors upon request (liuxianfeng7987@163.com).

Author contributions

XL and XF conceived and designed the research, XL conducted the experiments and analysed the results, XL wrote the manuscript with contributions from XF, CP and BF.

Competing interests

The authors declare that they have no conflict of interest.

References

Bergmann, I., Ramillien, G., and Frappart, F.: Climate-driven interannual ice mass evolution in Greenland. Global Planet Change, 82-83, 1-11, doi.org/10.1016/j.gloplacha.2011.11.005, 2012.

Brun, F., Berthier, E., and Wagnon, P.: A spatially resolved estimate of High Mountain Asia glacier mass balances from 2000 to 2016. Nat. Geosci., 10(9): 668-673, doi:10.1038/ngeo2999, 2017.

Cao, Q., Clark, E. A., and Mao, Y. X.: Trends and Interannual Variability in Terrestrial Water Storage Over the Eastern United States, 2003–2016. Water Resour. Res., 55(3): 1928-1950, doi:10.1029/2018wr023278, 2019.

Cleveland, R. B., Cleveland, W. S., and Mcrae, J. E.: STL: A Seasonal-Trend Decomposition Procedure Based on Loess. J. Off. Stat., 6(1): 3-73, 1990.

Crétaux, J. F., Jelinski, W., and Calmant, S.: SOLS: A lake database to monitor in the Near Real Time water level and storage variations from remote sensing data. Adv. Space Res., 47(9): 1497-1507, doi.org/10.1016/j.asr.2011.01.004, 2011.

345 Creutzfeldt, B., Heinrich, I., and Merz, B.: Total water storage dynamics derived from tree-ring records and terrestrial gravity observations. J. Hydrol., 529: 640-649, doi.org/10.1016/j.jhydrol.2015.04.006, 2015.

Du, Y., Xie, S. P., and Huang, G.: Role of Air–Sea Interaction in the Long Persistence of El Niño–Induced North Indian Ocean Warming. J. Climate, 22(8): 2023-2038, doi.org/10.1175/2008JCLI2590.1, 2009.

Famiglietti, J. S. and Rodell, M.: Water in the Balance. Science, 340(6138): 1300-1301, doi: 10.1126/science.1236460, 2013.

350 Feng, W., Shum, C., and Zhong, M.: Groundwater Storage Changes in China from Satellite Gravity: An Overview. Remote Sens., 10(5): 674, doi:10.3390/rs10050674, 2018.

Feng, W., Zhong, M., and Lemoine, J. M.: Evaluation of groundwater depletion in North China using the Gravity Recovery and Climate Experiment (GRACE) data and ground-based measurements. Water Resour. Res., 49(4): 2110-2118, doi: 10.1002/wrcr.20192, 2013.

355 Gonsamo, A., Chen, J. M., and Lombardozzi, D.: Global vegetation productivity response to climatic oscillations during the satellite era. Global Change Biol., 22: 3414-3426, doi.org/10.1111/gcb.13258, 2016.

Huang, J. P., Yu, H. P., and Guan, X. D.: Accelerated dryland expansion under climate change. Nat. Clim. Change, 6(2): 166-171, doi: 10.1038/nclimate2837, 2016.

Humphrey, V., Gudmundsson, L., and Seneviratne, S. I.: Assessing Global Water Storage Variability from GRACE: Trends, 360 Seasonal Cycle, Subseasonal Anomalies and Extremes. Surv. Geophys., 37(2): 357-395, doi: 10.1007/s10712-016-9367-1, 2016.

Humphrey, V., Zscheischler, J., and Ciais, P.: Sensitivity of atmospheric CO2 growth rate to observed changes in terrestrial water storage. Nature, 560(7720): 628-631, doi: 10.1038/s41586-018-0424-4, 2018.

Huss, M., and Hock, R.: Global-scale hydrological response to future glacier mass loss. Nat. Clim. Change, 8(2): 135-140, 365 doi: 10.1038/s41558-017-0049-x, 2018.

Jacob, T., Wahr, J., and Pfeffer, W.: Recent contributions of glaciers and ice caps to sea level rise. Nature, 482: 514-518, doi: 10.1038/nature10847, 2012.

Joodaki, G., Wahr, J., and Swenson, S.: Estimating the human contribution to groundwater depletion in the Middle East, from GRACE data, land surface models, and well observations. Water Resour. Res., 50(3): 2679-2692, doi: 370 10.1002/2013wr014633, 2014.

Kendall, M. G.: Rank correlation methods. London: Griffin, 1955.

Long, D., Chen, X., and Scanlon, B. R.: Have GRACE satellites overestimated groundwater depletion in the Northwest India Aquifer? Sci. Rep., 6(1): 24398, doi:10.1038/srep24398, 2016.

Long, D., Scanlon, B. R., and Longuevergne, L.: GRACE satellite monitoring of large depletion in water storage in response
375   to the 2011 drought in Texas. Geophys. Res. Lett., 40(13): 3395-3401, doi: 10.1002/grl.50655, 2013.

Long, D., Yang, Y. T., and Wada, Y.: Deriving scaling factors using a global hydrological model to restore GRACE total
water storage changes for China's Yangtze River Basin. Remote Sens. Environ., 168: 177-193, doi:org/10.1016/j.rse.2015.07.
003, 2015.

Meng, F., Su, F., and Li, Y.: Changes in Terrestrial Water Storage During 2003–2014 and Possible Causes in Tibetan
380   Plateau. J. Geophys. Res.-Atmos., 124(6): 2909-2931, doi: 10.1029/2018JD029552, 2019.

Ndehedehe, C. E., Awange, J. L., and Kuhn, M.: Climate teleconnections influence on West Africa's terrestrial water storage.
Hydrol. Process., 31(18): 3206-3224, doi:org/10.1002/hyp.11237, 2017.

Ni, S. N., Chen, J. L., and Wilson, C. R.: Global Terrestrial Water Storage Changes and Connections to ENSO Events. Surv.
Geophys., 39(1): 1-22, doi: 10.1007/s10712-017-9421-7, 2018.

385   Oppenheim, A. V., and Schafer, R. W.: Discrete-Time Signal Processing, 2009.

Panda, D. K. and Wahr, J.: Spatiotemporal evolution of water storage changes in India from the updated GRACE-derived
gravity records. Water Resour. Res., 52(1): 135-149, doi: 10.1002/2015wr017797, 2016.

Phillips, T., Nerem, R. S., and Fox-Kemper, B.: The influence of ENSO on global terrestrial water storage using GRACE.
Geophys. Res. Lett., 39, L16705, doi: 10.1029/2012GL052495, 2012.

390   Reager, J. T. and Famiglietti, J. S.: Global terrestrial water storage capacity and flood potential using GRACE. Geophys. Res.
Lett., 36(23), doi: 10.1029/2009GL040826, 2009.

Rodell, M., Chao, B. F., and Au, A. Y.: Global Biomass Variation and Its Geodynamic Effects: 1982–98. Earth Interact.,
9(2): 1-19, doi: org/10.1175/EI126.1, 2005.

Rodell, M., Famiglietti, J. S., and Wiese, D. N.: Emerging trends in global freshwater availability. Nature, 557: 651-659, doi:
395   10.1038/s41586-018-0123-1, 2018.

Rodell, M., Houser, P. R., and Jambor, U.: The Global Land Data Assimilation System. B. Am. Meteorol. Soc., 85(3): 381-
394, doi: 10.1175/bams-85-3-381, 2004.

Rodell, M., Velicogna, I., and Famiglietti, J. S.: Satellite-based estimates of groundwater depletion in India. Nature,
460(7258): 999-1002, doi: 10.1038/nature08238, 2009.

400   Salmon, J. M., Friedl, M. A., and Frolking, S.: Global rain-fed, irrigated, and paddy croplands: A new high resolution map
derived from remote sensing, crop inventories and climate data. Int. J. Appl. Earth Obs., 38: 321-334, doi:
10.1016/j.jag.2015.01.014, 2015.

Save, H, Bettadpur, S, and Tapley, B. D.: High-resolution CSR GRACE RL05 mascons. J. Geophys. Res.: Sol Ea, 121(10):
7547-7569, doi: 10.1002/2016jb013007, 2016.

405   Scanlon, B. R., Zhang, Z. Z., and Save, H.: Global evaluation of new GRACE mascon products for hydrologic applications.
Water Resour. Res., 52(12): 9412-9429, doi: 10.1002/2016wr019494, 2016.

Schwatke, C., Dettmering, D., and Bosch, W.: DAHITI – an innovative approach for estimating water level time series over inland waters using multi-mission satellite altimetry. Hydrol. Earth Syst. Sc., 19(10): 4345-4364, doi: 10.5194/hess-19-4345-2015, 2015.

410 Sen, P. K., Estimates of the regression coefficient based on Kendall's tau. J. Am. Stat. Assoc., 63(324): 1379-1389, 1968.

Shamsudduha, M. and Panda, D. K.: Spatiotemporal changes in terrestrial water storage in the Himalayan river basins and risks to water security in the region: A review. Int. J. Disast. Risk Re., 35: 101068, doi: 10.1016/j.ijdrr.2019.101068, 2019.

Shamsudduha, M., Taylor, R. G., and Jones, D.: Recent changes in terrestrial water storage in the Upper Nile Basin: an evaluation of commonly used gridded GRACE products. Hydrol. Earth Syst. Sc., 21(9): 4533-4549, doi: 10.5194/hess-21-

415 4533-2017, 2017.

Sherwood, S. and Fu, Q.: A Drier Future? Science, 343: 737-739, doi: 10.1126/science.1247620, 2014.

Sun, Z. L., Zhu, X. F., and Pan, Y. Z.: Drought evaluation using the GRACE terrestrial water storage deficit over the Yangtze River Basin, China. Sci. Total Environ., 634: 727-738, doi: 10.1016/j.scitotenv.2018.03.292, 2018.

Syed, T. H., Famiglietti, J. S., and Rodell, M.: Analysis of terrestrial water storage changes from GRACE and GLDAS.

420 Water Resour. Res., 44(2), doi: 10.1029/2006wr005779, 2008.

Tang, Q. H., Gao, H. L., and Yeh, P.: Dynamics of Terrestrial Water Storage Change from Satellite and Surface Observations and Modeling. J. Hydrometeorol., 11(1): 156-170, doi: 10.1175/2009jhm1152.1, 2010.

Tapley, B. D., Watkins, M. M., and Flechtner, F.: Contributions of GRACE to understanding climate change. Nat. Clim. Change, 9(5): 358-369, doi: 10.1038/s41558-019-0456-2, 2019.

425 Thomas, A. C., Reager, J. T., and Famiglietti, J. S.: A GRACE-based water storage deficit approach for hydrological drought characterization. Geophys. Res. Lett., 41(5): 1537-1545, doi: 10.1002/2014GL059323, 2014.

Thomas, B. F., Famiglietti, J. S., and Landerer, F. W.: GRACE Groundwater Drought Index: Evaluation of California Central Valley groundwater drought. Remote Sens. Environ., 198: 384-392, doi: 10.1016/j.rse.2017.06.026, 2017.

Voss, K. A., Famiglietti, J. S., and Lo, M. H.: Groundwater depletion in the Middle East from GRACE with implications for

430 transboundary water management in the Tigris-Euphrates-Western Iran region. Water Resour. Res., 49: 904-914, doi: 10.1002/wrcr.20078, 2013.

Wada, Y., van Beek, L. P. H., and van Kempen, C. M.: Global depletion of groundwater resources. Geophys. Res. Lett., 37: L20402, doi: 10.1029/2010GL044571, 2010.

Wallace, J. M. and Gutzler, D. S.: Teleconnections in the Geopotential Height Field during the Northern Hemisphere Winter.

435 Mon. Weather Rev., 109: 784-812, 1981.

Wang, J. D., Song, C. Q., and Reager, J. T.: Recent global decline in endorheic basin water storages. Nat. Geosci., 11(12): 926-932, doi: 10.1038/s41561-018-0265-7, 2018.

Wang, J. X., Huang, J. K., and Blanke, A.: The Development, Challenges and Management of Groundwater in Rural China. In Groundwater in Developing World Agriculture: Past, Present and Options for a Sustainable Future; Giordano, M., Shah,

440 T., Eds.; International Water Management Institute: Colombo, Sri Lanka: 37-62, 2007.

Watkins, M. M., Wiese, D. N., and Yuan, D. N.: Improved methods for observing Earth's time variable mass distribution with GRACE using spherical cap mascons. J. Geophys. Res.-sol. Ea., 120(4): 2648-2671, doi: 10.1002/2014jb011547, 2015.

Webster, P. J., Moore, A. M., and Loschnigg, J. P.: Coupled ocean-atmosphere dynamics in the Indian Ocean during 1997-98. Nature, 401: 356-360, 1999.

445 Yang, P., Xia, J., and Zhan, C. S.: Monitoring the spatiotemporal changes of terrestrial water storage using GRACE data in the Tarim River basin between 2002 and 2015. Sci. Total Environ., 595: 218-228, doi:10.1016/j.scitotenv.2017.03.268, 2017.

Yi, H. and Wen, L. X.: Satellite gravity measurement monitoring terrestrial water storage change and drought in the continental United States. Sci. Rep., 6: 19909, doi: 10.1038/srep19909, 2016.

Zhang, G. Q., Yao, T. D. and Piao, S. L.: Extensive and drastically different alpine lake changes on Asia's high plateaus
450 during the past four decades. Geophys. Res. Lett., 44(1): 252-260, doi: 10.1002/2016GL072033, 2017.

Zhang, G. Q., Yao, T. D. and Xie, H. J.: Increased mass over the Tibetan Plateau: From lakes or glaciers? Geophys. Res. Lett., 40(10): 2125-2130, doi: 10.1002/grl.50462, 2013.

Zhang, Z. Z., Chao, B. F., and Chen, J. L.: Terrestrial water storage anomalies of Yangtze River Basin droughts observed by GRACE and connections with ENSO. Global Planet. Change, 126: 35-45, doi: 10.1016/j.gloplacha.2015.01.002, 2015.

455 Zhu, Z. C., Piao, S. L., and Xu, Y. Y.: The effects of teleconnections on carbon fluxes of global terrestrial ecosystems. Geophys. Res. Lett., 44(7): 3209-3218, doi: 10.1002/2016GL071743, 2017.

460
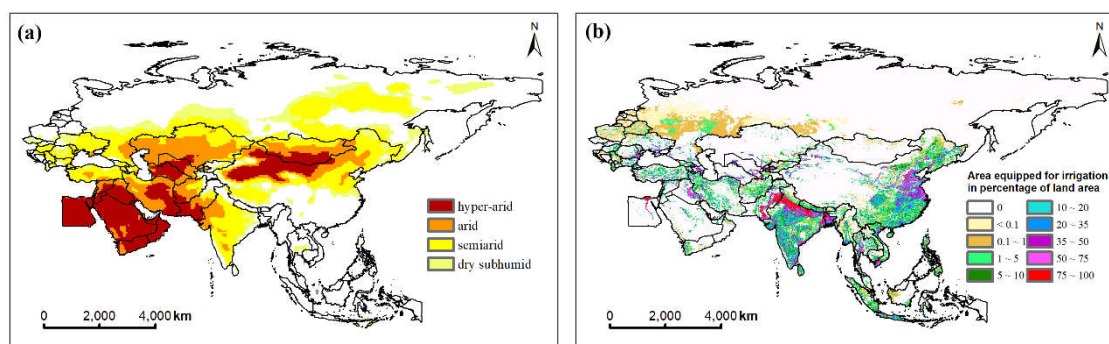
Figure 1: Boundary of the Asian and Eastern European regions. Panel (a) is the arid and semiarid distribution, and panel (b) is the percentage area of irrigated land across the study area.
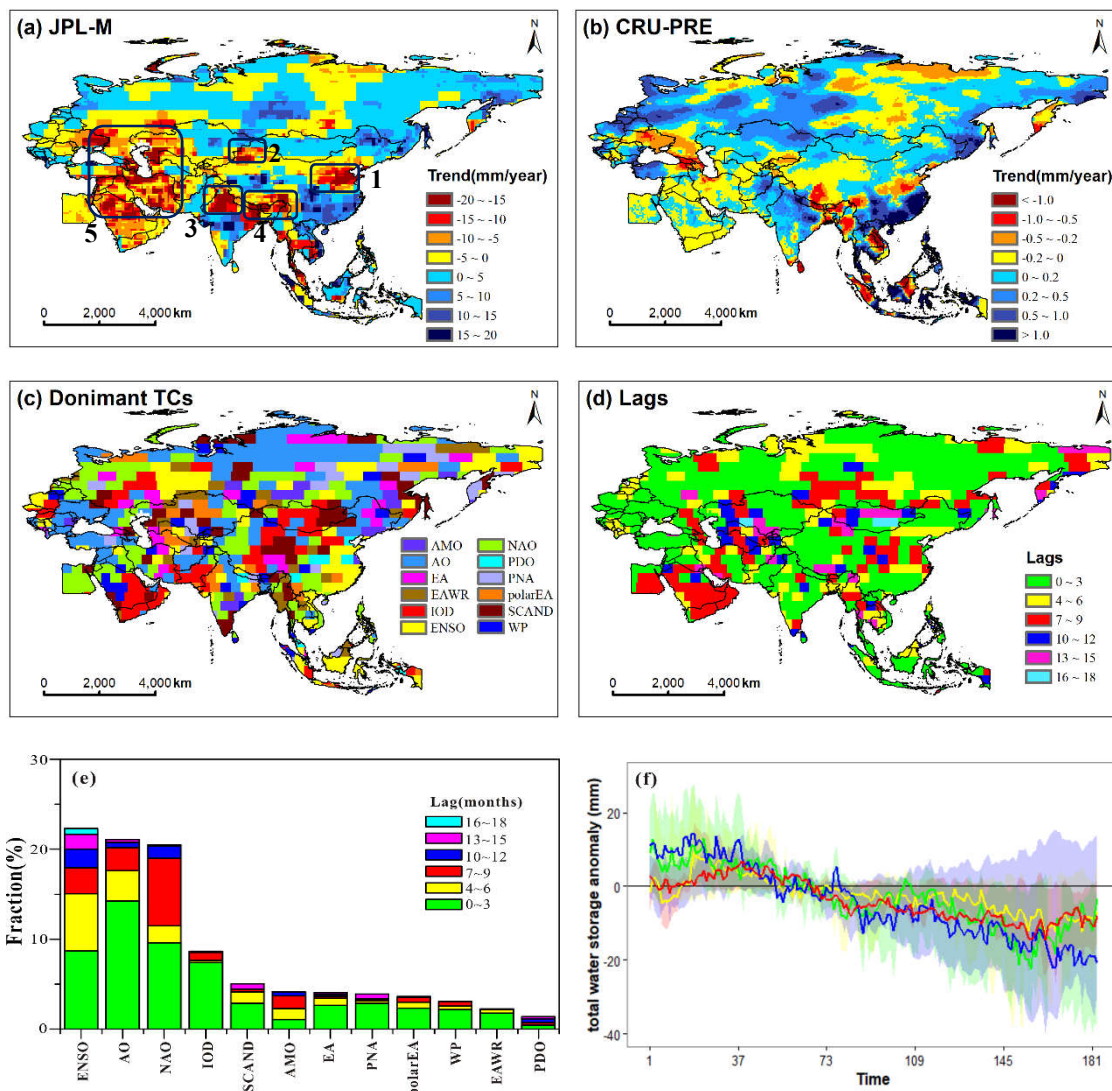
Figure 2: Spatiotemporal changes in TWS as obtained from GRACE (a) and precipitation as obtained from CRU (b) across the Asian and Eastern European regions during 2002-2017. The trend is obtained from the removed seasonal cycle time series. (c) Spatial pattern of teleconnections that can best represent TWS variations. (d) Spatial pattern of teleconnection lag time. The maximum phase shift in the correlation analysis was limited to 0~24 months (significance threshold: |r| > ~0.15 given α = 0.05 and n = 183). (e) Proportion of the global vegetated area dominated by each teleconnection and its corresponding time lags. (f) Changes in TWS across five hotspots. Uncertainties represent the 95% confidence intervals.
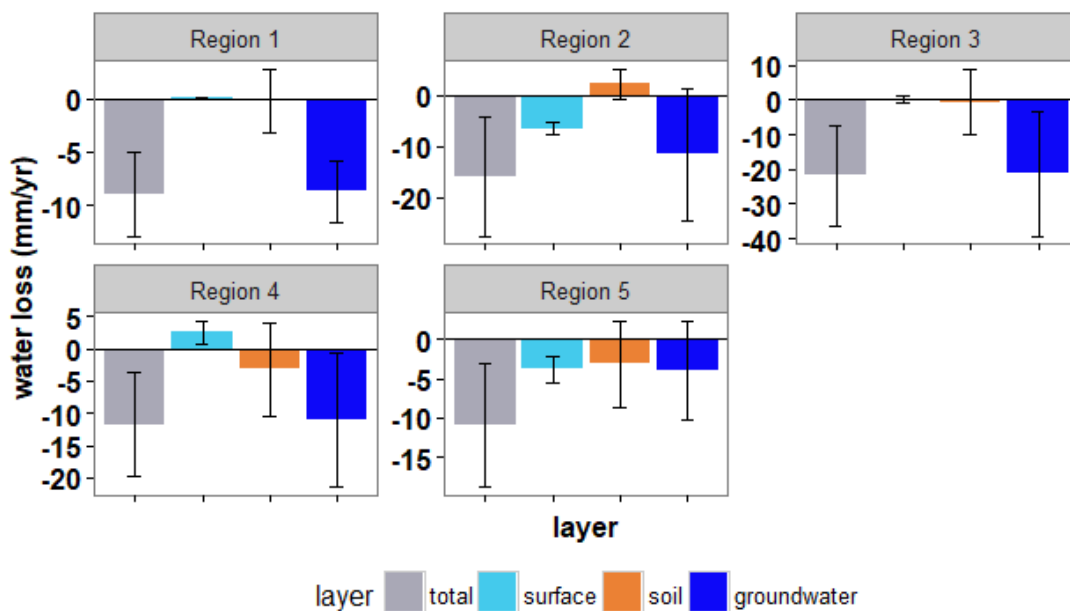
Figure 3: Contributions of different hydrological storages to TWS changes in five hotspots. Uncertainties represent the 95% confidence intervals.
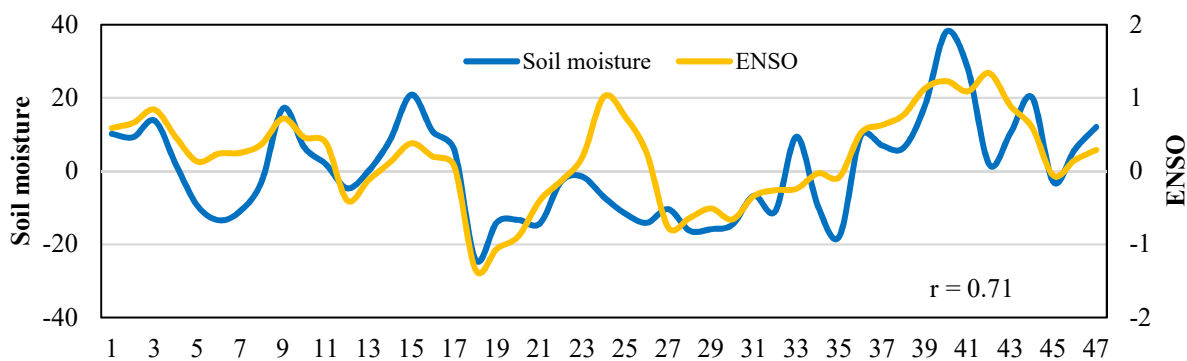
Figure 4: The residual time series of SM and associated ENSO in region 3 during the spring of the study period.